Enhanced Acoustic Pressure Sensors based on Coherent Perfect Absorber-Laser Effect

M. Farhat,[1,*] A. Khelif,[2] W. W. Ahmad,[1] K. N. Salama,[3] and Y. Wu[1]

[1]*Computer, Electrical, and Mathematical Science and Engineering (CEMSE) Division, King Abdullah University of Science and Technology (KAUST), Thuwal 23955-6900, Saudi Arabia*
[2]*Institut FEMTO-ST, CNRS, Universite de Bourgogne Franche-Comte, 25000 Besancon, France*
[3]*Sensors Lab, Advanced Membranes Porous Materials Center (AMPMC), Computer, Electrical and Mathematical Science and Engineering (CEMSE) Division, King Abdullah University of Science and Technology (KAUST), Thuwal 23955, Saudi Arabia*

(Dated: November 29, 2020)

Lasing in optical systems is a well-established field of research with several applications. Yet, having lasing or hugely amplifying systems for other wave domains remains an elusive goal. With the proposition of coherent perfect absorber-laser concept, we aim here to realize the first of its kind acoustic equivalent of laser, with a proven amplification of more than 10^4 in terms of the scattered acoustic signal, at frequency of a few kHz. The obtained acoustic laser (or CPA-Saser) is shown to possess extremely high sensitivity and figure of merit with regards to ultra-small variations of the pressure (density and compressibility) and suggests its evident potential to build future acoustic pressure devices such as precise sensors.

I. INTRODUCTION

The field of acoustic metamaterials started with the seminal work of P. Sheng on locally sonic materials [1]. Since then, a new community in physics was born, i.e., acoustical metamaterials and metasurfaces [2]. The main aim was to build new materials to control and tailor sound propagation and its interaction with matter in an unprecedented manner. Several innovative applications were put forward by this community, ranging from negative refraction [3], lensing [4, 5], transformation acoustics and cloaking [6] for the first act. The second act witnessed the birth of acoustic metasurfaces [7–9]: Several disruptive applications were proposed such as Parity-Time ($\mathscr{P}\mathscr{T}$) symmetry and non-reciprocal propagation [10–12], topological acoustics [13–15], enhanced sensing [11], Fano resonators [16, 17], or sound perfect absorption [18, 19] and insulation of buildings [20, 21].

In the same vein, the re-discovery of non-Hermitian Hamiltonian operators, and of quantum systems exhibiting Parity-Time ($\mathscr{P}\mathscr{T}$)-symmetry has given rise to several new physical and technological applications. The transposition to nanophotonics and other wave systems takes a particularly attractive form, insofar as the initial time-dependent Schrödinger equation is simply replaced by an equation of spatial wave evolution, along the axis of propagation. In fact, $\mathscr{P}\mathscr{T}$-symmetric operators have been initially proposed as an alternative to self-adjoint operators in quantum physics. The reality of the spectrum is then important from the point of view of physics. For instance, the spectacular feature of the $\mathscr{P}\mathscr{T}$-symmetric system is the unidirectional wave propagation at exceptional point (EP) that stems from the coalescence of the eigenspectrum [22, 23]. Most of the intriguing physical phenomena such as unidirectional invisibility [24], electromagnetic teleportation [25], Bloch oscillations [26], negative refraction [27], and field localization [28] are owed to singular characteristics of the EP. Quite interestingly, and as was done for some other wave phenomena, $\mathscr{P}\mathscr{T}$-symmetry and EPs were demonstrated for acoustic waves. The used structures were similar to those in optics, but here the balance of gain and loss is enforced to mass density. Soon after this theoretical propositions, the concept was subsequently verified, along with some intriguing applications, e.g., acoustic invisible sensors, signal manipulation, cloaking, or beam splitting.

Recently, a new kind of singularity associated to the CPA-laser (coherent perfect absorber-laser: CPAL) effect gained substantial attention in the field of $\mathscr{P}\mathscr{T}$-symmetric Optics [29]. CPA-lasers exhibit eigenvalues to be either zero or infinity, which allows for coherent perfect absorption and lasing, altogether. This peculiar behavior was shown to possess unprecedented features, especially in the realm of electronics where loss and gain were realized using positive and negative resistors, respectively [30]. In particular, the CPAL was employed as method to enhance the sensitivity of radio-frequency sensors by operating a $\mathscr{P}\mathscr{T}$-symmetric system at its CPAL point [30, 31]. Degeneracies in non-Hermitian systems have attracted much attention for sensing applications owing to their potential to amplify the system response to a small perturbation, yet the means of measuring the system's spectral response and the associated effects of noise are still challenging tasks [31, 32]. By translating the CPAL concept into acoustic systems, we can observe similar singularity in $\mathscr{P}\mathscr{T}$-symmetric acoustics i.e., CPA-Saser. Saser [33] is analogous to laser in acoustic domain, which may exhibit perfect absorption and amplification around CPAL point for the acoustic waves. Hence, by exploiting transitions between acoustic absorption and acoustic lasing at a CPAL point, we could demonstrate that small perturbations can be translated into large changes in the output intensity (which may be easily detectable), provided that the phase between two coherent input waves can be precisely controlled.

In this work, we propose a CPAL-based acoustic sensing platform, composed of three thin-layers, where the passive layer is sandwiched between gain and loss layers. The arrangement of acoustic materials with complex parameters (gain/loss) determines the existence of CPLA point in the proposed sensor to induce ultrahigh sensitivity for the inci-

* mohamed.farhat@kaust.edu.sa

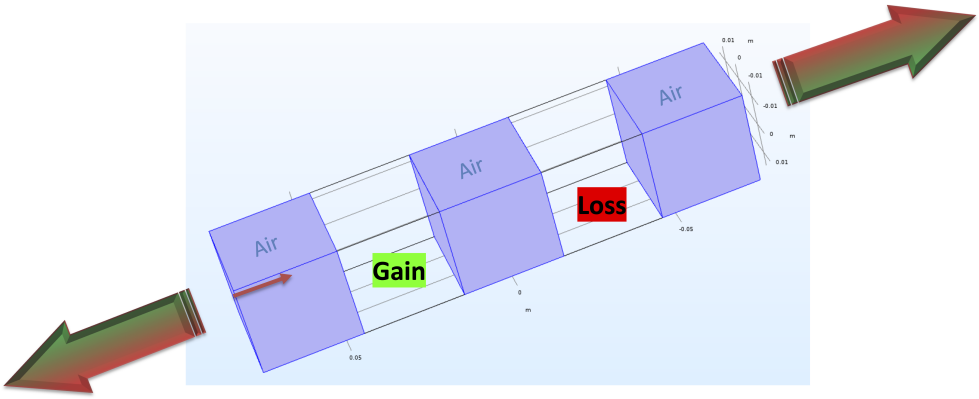

Figure 1. Schematic representation of the sensing acoustic device, based on the $\mathscr{P}\mathscr{T}$-symmetry breaking and the CPAL effect. The thin arrow represents the exciting acoustic signal of unit-amplitude, whereas the thick arrows indicate the huge reflection and transmission (outgoing signals), around the coherent perfect absorber-laser (CPAL) frequency. The thickness of all three layers is taken to be 3 cm. The density of gain/loss is $\rho_0(1\mp 0.75i)$ and its compressibility is taken to be equal to that of air β_0, with $\rho_0 = 1.29$ kg/m^3 the density of air.

dent acoustic waves. The remaining of this paper is organized as follows. In Section II, we provide the background and mathematical formulation of the acoustic CPAL effect through $\mathscr{P}\mathscr{T}$-symmetry in the context of a multi-layered structure. Section III gives the main results of this work: Sub-section III A details the origin of acoustic CPAL and its intriguing scattering properties, while sub-section III B details the sensing mechanism and its robustness to detect small background pressure variation. Finally, Section IV gives some concluding remarks.

II. MATERIALS AND METHODS

The equations governing the propagation of acoustic (pressure) waves in the limit of small perturbation in incompressible and inviscid fluids can be derived from the momentum and mass conservation equations of fluids at rest [34], i.e.,

$$\rho\frac{\partial \mathbf{u}}{\partial t} = -\nabla p\,, \qquad \beta\frac{\partial p}{\partial t} = -\nabla\cdot\mathbf{u}\,, \tag{1}$$

where ρ denotes the density and β is the compressibility of the background medium (here $\beta = 1/\kappa$, with κ the bulk modulus of the medium). These equations are complemented by the continuity of the normal component of the velocity field $\mathbf{n}\cdot\mathbf{u}$, with $\mathbf{n}$ the normal unit vector to the considered boundary as well as the pressure field p.

The system of Eq. (1) leads to the wave equation (assuming piece-wise homogeneous physical properties)

$$\nabla^2 p - \frac{1}{c^2}\frac{\partial^2 p}{\partial t^2}\,, \tag{2}$$

where $1/c^2 = \rho\beta$ is the speed of sound in the given medium. As mentioned earlier, this equation is valid for relatively small pressure perturbation. The structures that we will consider in this study are multi-layered (with one dimension infinitely extended) as can be seen from Fig. 1, as example. Hence, a convenient transfer matrix formalism is developed for this purpose, to compute the transmitted and reflected signals (arrows of Fig. 1) and is compared to the results from finite elements method (FEM, from Comsol Multiphysics [35]). Moreover, Fig. 1 shows layers with alternating gain and loss (positive/negative imaginary parts in the mass density, assuming a time-harmonic dependence of $e^{-i\omega t}$) as this is needed to achieve the so-called parity-time ($\mathscr{P}\mathscr{T}$)-symmetry and the subsequent exceptional point (EP) when this symmetry is broken at specific points in the spectral regime.

This effect was already proposed both theoretically and experimentally in the realm of pressure waves. But in order to set up our problem we wish to re-emphasize some key points and notations. First, the scattering matrix relating the outgoing (scattered) signals to the incoming (incident) ones, can be expressed as

$$S(\omega) = \begin{pmatrix} t & r_R \\ r_L & t \end{pmatrix}, \tag{3}$$

with t the transmission coefficient (identical in both incidences, due to reciprocity), r_R and r_L are the reflection coefficients from right and left incidences, respectively. All these coefficients are complex valued, and they obey the energy conservation relation

$$tt^* + r_L r_R^* = t^* t + r_L^* r_R = 1\,. \tag{4}$$

It is evident from Eq. (4) that if $tt^* = T = 1$, the product $r_L r_R = 0$, which can be satisfied if r_L and/or r_R is zero, and no need for the remaining coefficient to vanish, demonstrating the possibility of asymmetric reflectionless operation [30].

III. RESULTS

A. $\mathscr{P}\mathscr{T}$-symmetry and CPAL Effect

As shown in Ref. [10], when $T > 1$, r_R and r_L are π out of phase, while they are in phase for $T < 1$. It was further

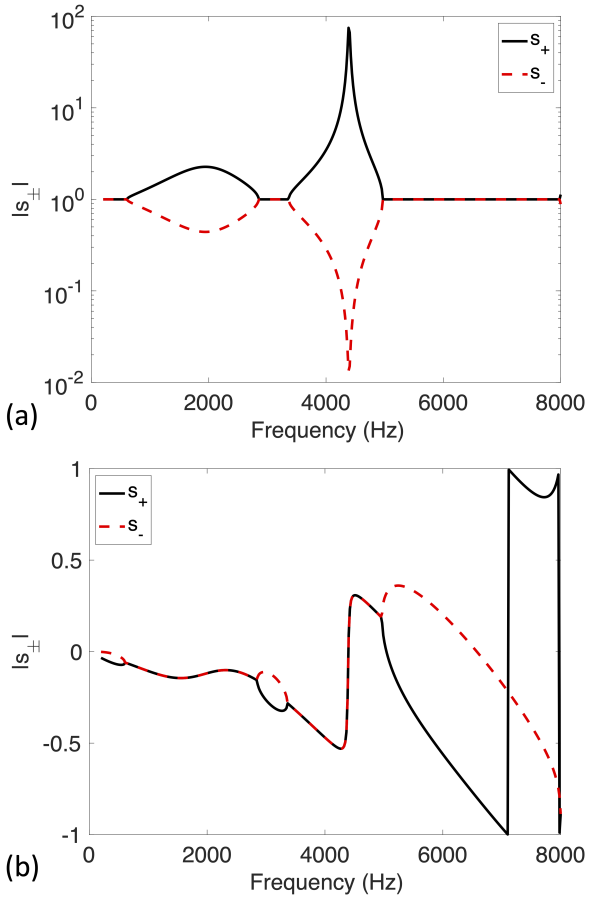

Figure 2. (a) Eigenvalue amplitude for the same structure as of Fig. 1, showing lasing and coherent perfect absorber effect at frequency around 4383 kHz. (b) Phase of the eigenvalues $s_\pm$ normalized by π.

shown that the $\mathscr{P}\mathscr{T}$-symmetric (or exact) phase corresponds to $T<1$, while the broken phase is obtained for $T>1$. The transition between these two phases occurs when $T=1$, at the so-called EP. In order to quantitatively characterize this $\mathscr{P}\mathscr{T}$-symmetry effects, we need to compute the eigenvalues of the S-matrix given in Eq. (3), that we should coin $s_\pm$, which are given by

$$s_\pm(\omega) = t \mp \sqrt{r_L r_R} = t\left(1 \mp i\sqrt{\frac{1-T}{T}}\right). \qquad (5)$$

Thus, when $T<1$, $s\pm$ are complex-conjugate, i.e., are unit-modular ($|s_\pm|=1$). For $T>1$ (the broken phase), $s_\pm$ have different modulus, namely $|s_\pm| = \sqrt{T}(1\pm\sqrt{1-1/T})$. The amplitude of these eigenvalues is given in Fig. 2(a) as well as their phases in Fig. 2(b). The highlighted regions (in yellow) stand for the broken phase. The low frequency region spanning frequencies XX-XX Hz describes regular EP and $\mathscr{P}\mathscr{T}$-symmetry breaking. This behavior is confirmed in Figs. 3(a)-(b) where the T/R spectra is plotted, and where a zero left reflection can be observed around XX kHz. Yet, we know that using gain/loss media, above certain threshold may result in another related effect, namely coherent perfect absorber-laser (CPAL) reminiscent of a singular point in the spectrum. In fact, as can be seen in Fig. 2, at frequency $f=4.383$ kHz, one of the eigenvalues s_+, diverges (plot in logarithmic scale) as shown by the black line, while the second eigenvalue s_-, vanishes as shown by the dashed red line. s_+ thus corresponds to lasing while s_- corresponds to coherent perfect absorption (CPA). From inspection of the scattering matrix of Eq. (3) and the incoming (p_L^{in}, p_R^{in}) and outgoing pressure waves (p_L^{out}, p_R^{out}) we can easily derive the conditions of resonant scattering (amplification or lasing) and of CPA. For instance, for lasing to occur, we have to impose zero incoming signals, i.e., $p_L^{\text{in}}=p_R^{\text{in}}=0$ and finite outgoing ones, i.e., $p_L^{\text{out}}\approx p_R^{\text{out}}\approx 1$. By the use of the transfer matrix equation instead, i.e., $(p_L^{\text{in}}, p_L^{\text{out}})^T = M(p_R^{\text{out}}, p_R^{\text{in}})$, which leads to $m_{11}p_R^{\text{out}}=0$ and $m_{21}p_R^{\text{out}}=p_L^{\text{out}}$. Since we want finite scattering, this just means $m_{11}=0$ and $m_{21}=p_L^{\text{out}}/p_R^{\text{out}}$. Or, in other words, a condition on the M-matrix through its components m_{11} and m_{21}, that depend on the geometry and physical parameters of the structure, as well as on frequency. The second condition means that the outgoing waves are related to m_{21}, which is a free condition, as the outgoing signals cannot be controlled by the experiment setup, and rather just obey this condition (both amplitude and phase).

Let us move now to CPA operation occurring at the same frequency. We have to enforce in this case finite incident signals but zero outgoing ones, as all the energy has to be absorbed by the device in this operation regime. Namely, this leads to $m_{22}=0$ and $m_{12}=p_L^{\text{in}}/p_R^{\text{in}}$. The first condition is as before depending on the device itself, while the second, is here, of crucial difference, as it means that the incoming pressure waves (from both sides) should be tailored in both amplitude and phase, i.e., being coherent, as m_{12} is a complex number, i.e., $\phi(p_L^{\text{in}})=\phi(p_R^{\text{in}})+\phi(m_{12})$ and $|p_L^{\text{in}}|=|m_{12}||p_R^{\text{in}}|$. This shows that CPA is more stringent than lasing, that only requires $m_{11}=0$. Moreover, these two conditions should occur at the same frequency, which means that m_{11} m_{12} should vanish simultaneously for CPAL to take place. Hence, CPAL is a complex and rather more constrained effect than EP and $\mathscr{P}\mathscr{T}$-symmetry breaking.

In other words, since the S-matrix terms are inversely proportional to m_{22}, this shows that CPAL is equivalent to a pole (and a zero) in the S-matrix, that reflects into the eigenvalues $s_\pm$. These eigenvalues are plotted in Fig. 2(a)-(b) for the amplitude and phase, respectively. As per the structure we consider (shown in Fig. 1) CPAL occurs with same physical properties and geometry as before but for a higher frequency, i.e., around 4 kHz. As can be seen in Fig. 2(a), $s_\pm$ undergoes a resonance, reaching extremely high amplitude ($\approx 10^2$) by jumping from 1, i.e., the unit-modular or exact $\mathscr{P}\mathscr{T}$-symmetric phase. Thus, during this broken $\mathscr{P}\mathscr{T}$ phase, CPAL takes place. This fact is further demonstrated by the phase behavior around this point, i.e., $\phi(s_+)$ jumps from $-\pi/2$ to $\pi/2$, around the EP location. The CPA is described in Fig. 2(a) by the red curve that reaches a value near-zero at exactly the same frequency 4 kHz, and its phase undergoes similar jump. As we are interested about the practical applications of this feature, we define the output coefficient of the acoustic device as the

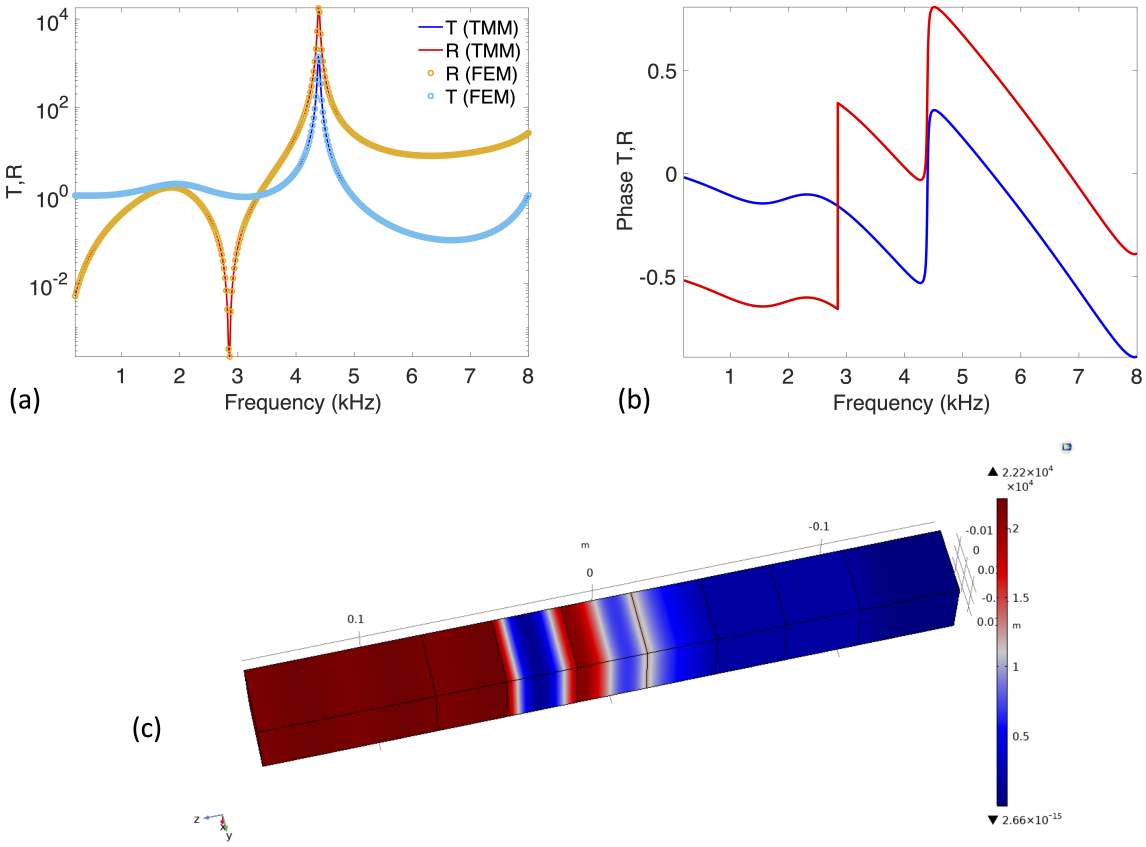

Figure 3. (a) Transmission and reflection spectrum of the structure shown in Fig. 1 in logarithmic scale, obtained using transfer matrix formalism (continuous lines) and using COMSOL software based on finite elements (dotted curves) in the frequency range 0.1-8 kHz. (b) Phase of the transmission reflection normalized by π showing the phase jump around CPAL frequency as well as around lower frequency EP. (c) Snapshots of the pressure field at lasing frequency 4.383 kHz, showing huge reflection and transmission, confirming lasing.

ratio between the outgoing energy divided by the ingoing one, i.e.,

$$\Psi = \frac{|p_L^{\text{out}}|^2 + |p_R^{\text{out}}|^2}{|p_L^{\text{in}}|^2 + |p_R^{\text{in}}|^2}. \tag{6}$$

If $\Psi = 0$, we have CPA, and if $\Psi \to \infty$ (or $\Psi \gg 1$), we have lasing. This coefficient is plotted in Fig. 3(a) along with transmission and reflection spectra. Around 4.38 kHz, Ψ diverges as expected for CPAL operation ($T \gg 1$ and $R \gg 1$, as demonstrated by both FEM simulations and TMM calculations). The phases of both t and r_L undergo jumps around the EP. The near-field pressure field is plotted in Fig. 3(c) at CPAL frequency, and its amplitude $|p|^2$ reaches extremely high values of 2.2 10^4 Pa for an incident wave of only 1 Pa, demonstrating the amplification (lasing) abilities of this $\mathscr{PT}$-based device. Here, it should be emphasized that $R \gg T$ ($\gg 1$). But, if we interchange the position of gain and loss layers (or equivalently switch from left incidence to right incidence) we will have $T > R$. But, due to reciprocity T must remain the same. And, hence the scenario shown in Fig. 3 is the best-suited for lasing as it provides the highest Ψ [See inset of Fig. 3(a)].

B. Acoustic Sensing

1. *Sensing Mechanism*

As can be clearly seen from Figs. 2 and 3, the resonance associated with the CPAL point from intertwined gain and loss possesses an extremely high Q-factor ($\approx 10^3$) that is important for sensing capabilities purposes. In order to use our device as acoustic sensor, we first investigate its output amplitude behavior, under small shifts of the density or compressibility of the surrounding, or of the middle passive layer (if the sensor is operated for non-destructive characterization). Figures 4(a) and 4(b) show the frequency responses of Ψ for the proposed sensor as functions of changes in $\Re(\rho_0)$ and $\Re(\beta_0^{-1})$, respectively. For the former case, $\Re(\rho_0)$ is varied between 1.29-1.889 kg/m^3 and in the latter $\Re(\beta_0^{-1})$ is varied between 0.1518-0.2222 MPa. Due to the extremely high Q-factor of the CPAL resonance and its extreme sensitivity, we can see that Ψ is greatly shifted, for small changes in the surrounding acoustical properties. In Fig. 4(a) we can observe a redshift, while in Fig. 4(b), a blueshift is observed with respect to increasing β_0^{-1} [yet, if we choose β_0, this corresponds actually to a redshift, too, as what matters really here, is the

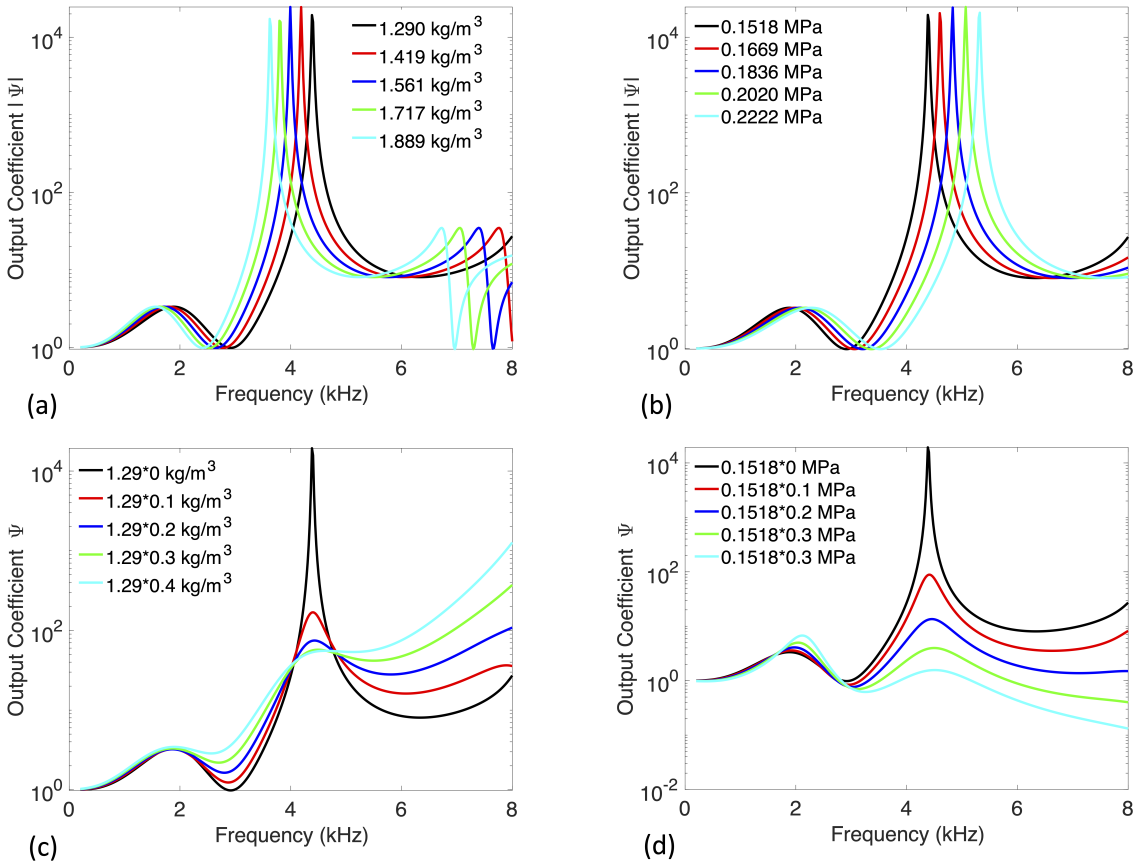

Figure 4. Amplitude of the output coefficient $|\Psi|$ for (a) varying real part of the density of the surrounding medium, (b) varying real part of the bulk modulus of the surrounding medium. (c) Same as in (a) but for the imaginary part of the density. (d) Same as in (b) but for the imaginary part of the bulk modulus.

acoustic refractive index, in analogy to refractive index sensing, if we define $n = \sqrt{\rho_r \beta_r}$, and the subscript r denotes relative quantity with respect to the surrounding]. These figures demonstrate the potential of CPAL acoustic sensors. It is instructive to check the effect of a change in the imaginary parts of ρ_0 and β_0, keeping their real parts constant, as in some scenarios, the presence of the analyte causes some absorption (change in imaginary parts). Figures 4(c) and 4(d) are the same as in Figs. 4(a) and 4(b) but for variation of the imaginary parts, instead. The main difference here is that there is no shift of the CPAL frequency, but the height of the resonance and its width (Q-factor) is dramatically reduced. So, sensing by scanning frequency shifts is not possible in this case. Let us move now to quantitative evaluation of the performance of the CPAL-based acoustic sensor in the reactive mode [$\Re(\rho_0)$]. To this end, we use the classical definition of sensitivity S and figure of merit (FoM), i.e.,

$$S = \frac{\Delta f\,(\mathrm{kHz})}{\Delta\left[\Re(\rho)\right](\mathrm{MDU})}, \tag{7}$$

and

$$FoM = \frac{S\,(\mathrm{kHz/MDU})}{FWHM\,(\mathrm{kHz})}. \tag{8}$$

S is thus the ratio of the unit change if the frequency (or more precisely the peak-shift in the CPAL resonance) for a unit change in $\Re(\rho_0)$ of the surrounding medium. The FoM is

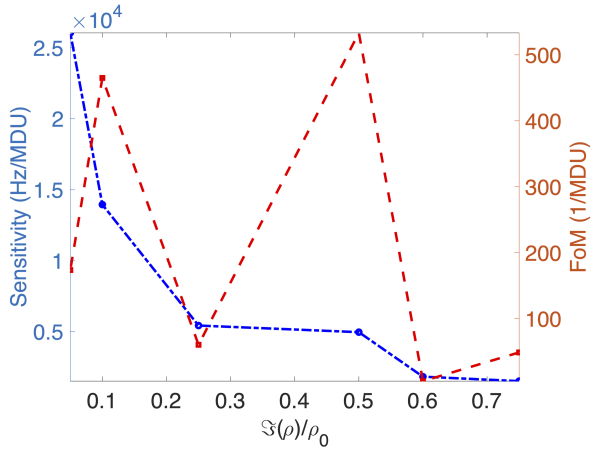

Figure 5. (Left axis) Acoustic sensitivity and (right axis) figure of merit (FoM) versus the imaginary part of the gain/loss layers (in units of the density of air).

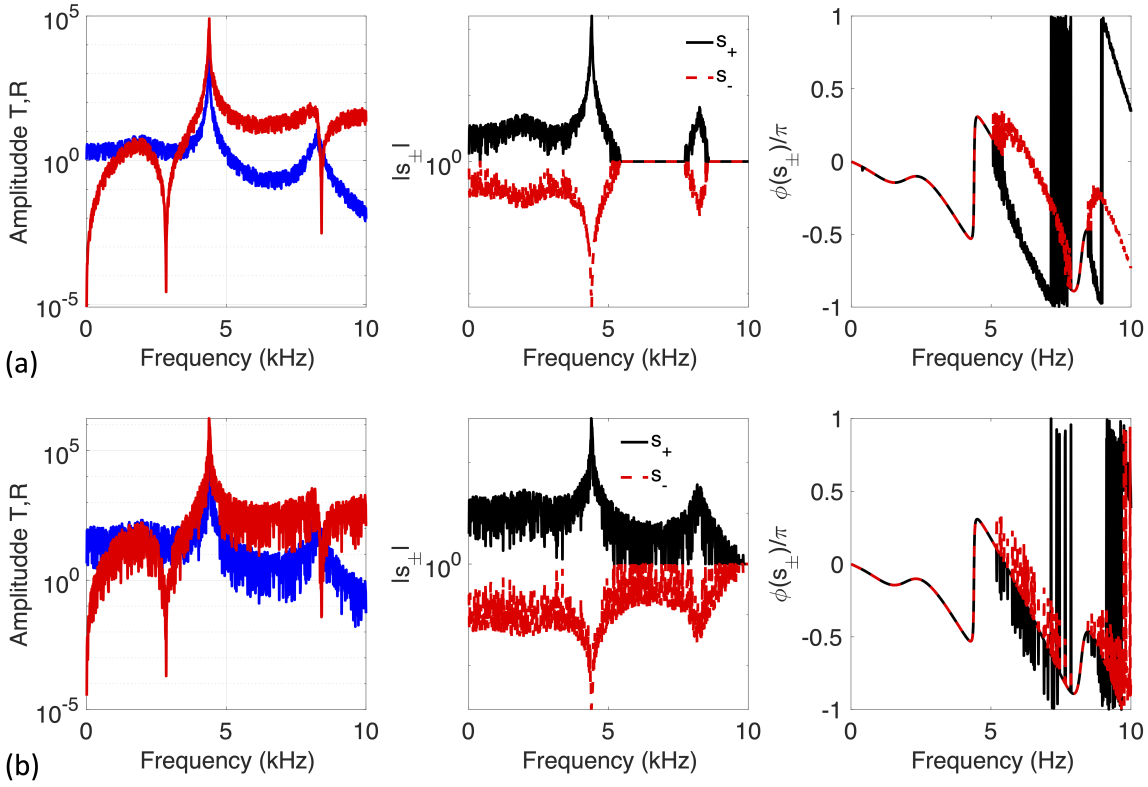

Figure 6. (a) (Left panel) Amplitude of the reflection and transmission spectra of the CPAL device, (middle panel) eigenvalue amplitude of $s_\pm$ versus frequency and (right panel) its phase, for a noise of 5 %. (b) Same as (a) but for a higher white noise level of 10 %.

another quantity that further and comprehensively evaluates the performance of the CPAL sensor. To have high *FoM*, not only *S* should be maximized, but also the *FWHM* should be minimized. Generally, these two extremums do not occur at the same frequency. So, a sort of trade-off should be sough for.

Figure 5 plots the main sensing parameters *S* and *FoM* versus the gain/loss parameters ($\Im(\rho)/\rho_0$, normalized with ρ_0, the density of the surrounding medium, here, air) from 0.05 to 0.75. The sensitivity *S* reaches extremely high values in the order of 10^4 Hz/MDU, with MDU referring to mass density unit, i.e., 1 kg/m^3. Hence, the smaller $\Im(\rho)$, the higher the resonance frequency f_0 and thus *S*. Therefore, if the interest is on CPAL sensing, as in our case, we should optimize *S* and *FoM*. This occurs, in our scenario, for $\Im(\rho)/\rho_0 = 0.1$. If the focus is on lasing (amplification) then higher gain/loss is needed to increase Ψ, but *S* is one order of magnitude lower, as can be seen in Fig. 5.

2. *Noise Effect*

Distinguishing signal changes caused by small perturbations from inevitable background noises is of paramount importance for acoustic sensor applications. We should point out that phase and flicker noises, which were reported to influence the performance and resolvability of EP-based sensors, may be insignificant in our proposed acoustic sensing platform [36, 37]. This is because a CPAL-based sensor detects power levels of scattered monochromatic waves at a fixed operating frequency, instead of tracking resonance frequency shifts due to eigenvalue bifurcation nearby the second- or higher-order EPs. As a result, phase and flicker noises, modal interference, and limited spectral density issues, which are regarded as relevant issues in EP-based sensors, can be addressed using the proposed new sensing paradigm.

In this paper, we mainly focus on demonstrating the ultra-high sensitivity and large modulation depth of CPAL-based acoustic (pressure) sensors. Hence, the noise level (including noise from the excitation sources, and auxiliary electric circuit) and spectral resolution (including the resolution of the tunability of excitation laser and the spectrometer) could not be acquired without an experimental implementation. Without loss of generality, only sensitivity (via the output coefficient Ψ) was calculated to evaluate the performance of the sensor. The effects of the background noise (dominantly contributed by the thermal noise) on the lower bound of sensing capability are displayed in Fig. 6, where two levels of white noise are enforced. We found that these levels of noise may have little effect on the performance of CPAL-locked PT-symmetric acoustic sensors, as evidenced by the persistence of the CPAL peak, that used to calculate the sensitivity.

IV. CONCLUDING REMARKS

A CPAl-based acoustic sensor using the paradigms of $\mathscr{P}\mathscr{T}$-symmetry breaking has been numerically investigated in this contribution. Compared with classical acoustic sensors, the CPAL sensor with only 3 layers (gain, loss, and passive) exhibited a much higher sensitivity in the order of 10^4 Hz per mass density unit. T our best knowledge, this is the first time that a CPAL acoustic sensors were reported. The obtained results show the potential of this device to improve acoustic sensors by balancing gain and loss.

ACKNOWLEDGEMENTS

The research reported in this manuscript was supported by King Abdullah University of Science and Technology (KAUST) Office of Sponsored Research (OSR) under Grant No. OSR-2016-CRG5-2950 and KAUST Baseline Research Fund BAS/1/1626-01-01.

DATA AVAILABILITY

The data that support the findings of this study are available from the corresponding author upon reasonable request.

REFERENCES

[1] Z. Liu, X. Zhang, Y. Mao, Y. Zhu, Z. Yang, C. T. Chan, and P. Sheng, science **289**, 1734 (2000).

[2] B. Assouar, "Preface to special topic: Acoustic metamaterials and metasurfaces," (2018).

[3] V. M. García-Chocano, J. Christensen, and J. Sánchez-Dehesa, Physical review letters **112**, 144301 (2014).

[4] K. Imamura and S. Tamura, Physical Review B **70**, 174308 (2004).

[5] R. V. Craster and S. Guenneau, *Acoustic metamaterials: Negative refraction, imaging, lensing and cloaking*, Vol. 166 (Springer Science & Business Media, 2012).

[6] G. Dupont, M. Farhat, A. Diatta, S. Guenneau, and S. Enoch, Wave Motion **48**, 483 (2011).

[7] Y. Li, B. Liang, Z.-m. Gu, X.-y. Zou, and J.-c. Cheng, Scientific reports **3**, 2546 (2013).

[8] Y. Xie, W. Wang, H. Chen, A. Konneker, B.-I. Popa, and S. A. Cummer, Nature communications **5**, 1 (2014).

[9] B. Assouar, B. Liang, Y. Wu, Y. Li, J.-C. Cheng, and Y. Jing, Nature Reviews Materials **3**, 460 (2018).

[10] X. Zhu, H. Ramezani, C. Shi, J. Zhu, and X. Zhang, Physical Review X **4**, 031042 (2014).

[11] R. Fleury, D. Sounas, and A. Alu, Nature communications **6**, 1 (2015).

[12] J. Christensen, M. Willatzen, V. Velasco, and M.-H. Lu, Physical review letters **116**, 207601 (2016).

[13] Z. Yang, F. Gao, X. Shi, X. Lin, Z. Gao, Y. Chong, and B. Zhang, Physical review letters **114**, 114301 (2015).

[14] X. Zhang, M. Xiao, Y. Cheng, M.-H. Lu, and J. Christensen, Communications Physics **1**, 1 (2018).

[15] J. Köpfler, T. Frenzel, M. Kadic, J. Schmalian, and M. Wegener, Physical Review Applied **11**, 034059 (2019).

[16] M. Amin, A. Elayouch, M. Farhat, M. Addouche, A. Khelif, and H. Bağcı, Journal of Applied Physics **118**, 164901 (2015).

[17] M. Amin, O. Siddiqui, M. Farhat, and A. Khelif, Journal of Applied Physics **123**, 144502 (2018).

[18] J. Mei, G. Ma, M. Yang, Z. Yang, W. Wen, and P. Sheng, Nature communications **3**, 1 (2012).

[19] M. D. Guild, V. M. García-Chocano, W. Kan, and J. Sánchez-Dehesa, Journal of Applied Physics **117**, 114902 (2015).

[20] A. Elayouch, M. Addouche, M. Farhat, M. Amin, H. Bağcı, and A. Khelif, EPL (Europhysics Letters) **116**, 46004 (2017).

[21] S. Kumar and H. P. Lee, in *Acoustics*, Vol. 1 (Multidisciplinary Digital Publishing Institute, 2019) pp. 590–607.

[22] C. E. Rüter, K. G. Makris, R. El-Ganainy, D. N. Christodoulides, M. Segev, and D. Kip, Nature physics **6**, 192 (2010).

[23] R. El-Ganainy, K. G. Makris, M. Khajavikhan, Z. H. Musslimani, S. Rotter, and D. N. Christodoulides, Nature Physics **14**, 11 (2018).

[24] M. Maldovan, Nature **503**, 209 (2013).

[25] S. Longhi, Physical review letters **103**, 123601 (2009).

[26] Y. Ra'di, D. Sounas, A. Alù, and S. Tretyakov, Physical Review B **93**, 235427 (2016).

[27] R. Fleury, D. L. Sounas, and A. Alu, Physical review letters **113**, 023903 (2014).

[28] W. Ahmed, R. Herrero, M. Botey, and K. Staliunas, Physical Review A **94**, 053819 (2016).

[29] S. Longhi, Physical Review A **82**, 031801 (2010).

[30] M. Sakhdari, M. Farhat, and P.-Y. Chen, New Journal of Physics **19**, 065002 (2017).

[31] M. Farhat, M. Yang, Z. Ye, and P.-Y. Chen, ACS Photonics **7**, 2080 (2020).

[32] Z. Xiao, H. Li, T. Kottos, and A. Alù, Physical Review Letters **123**, 213901 (2019).

[33] S. Zavtrak and I. Volkov, Technical Physics **42**, 406 (1997).

[34] P. M. Morse and K. U. Ingard, *Theoretical acoustics* (Princeton university press, 1986).

[35] "Comsol multiphysics® v. 5.4. www.comsol.com. comsol ab, stockholm, sweden.".

[36] N. A. Mortensen, P. Gonçalves, M. Khajavikhan, D. N. Christodoulides, C. Tserkezis, and C. Wolff, Optica **5**, 1342 (2018).

[37] M. Zhang, W. Sweeney, C. W. Hsu, L. Yang, A. Stone, and L. Jiang, Physical review letters **123**, 180501 (2019).

[38] M. Sakhdari, M. Hajizadegan, Y. Li, M. M.-C. Cheng, J. C. Hung, and P.-Y. Chen, IEEE Sensors Journal **18**, 9548 (2018).